Performance of the ATLAS semiconductor tracker

Cristiano Alpigiani[*][†]

Queen Mary University of London
E-mail: Cristiano.Alpigiani@cern.ch

We report the operation and performance of the ATLAS Semi-Conductor Tracker (SCT) functioning in a high luminosity and high radiation environment. The SCT, operating in the 2 T solenoidal magnetic field, is part of the inner tracking system of the ATLAS experiment at CERN and is designed to measure, for each track, at least four precise space points. The SCT is constructed of 4088 modules assembled from silicon-strip sensors for a total of 6.3 million channels more than 99 % of which were fully functional throughout all data taking periods. Noise occupancy and hit efficiency as well as the Lorentz angle and radiation damage measurements will be discussed in detail.

---

[*]Speaker.

[†]On behalf of the ATLAS Collaboration.

1. Introduction

The ATLAS (A Toroidal Lhc ApparatuS) detector [1, 2] is a general purpose experiment oper-
ating at the Large Hadron Collider (LHC) at CERN and it is divided in three main part components.
Moving outward from the interaction point, the detector consists of a tracking system able to mea-
sure the directions and momenta of the charged particles. The calorimeter system measures the
energies of the electrons, photons and hadrons. The muon spectrometer measures the momentum
and position of the muons that have enough energy to reach it. Furthermore, a magnet system pro-
vides a magnetic field, allowing the tracker and the muon spectrometer to perform measurements
of the momentum of charged particles.
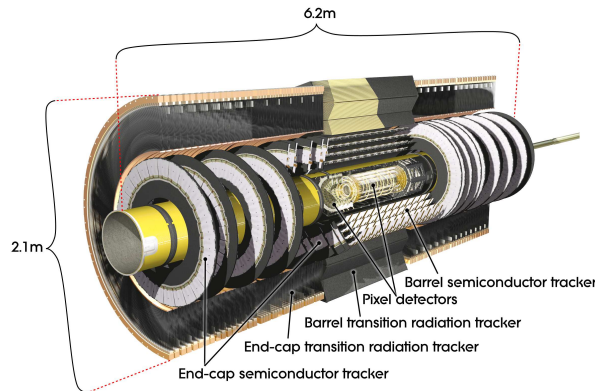
Figure 1: View of the ATLAS inner detector.

2. The ATLAS semiconductor tracker

The SCT [3] consists of four cylindrical layers (referred to as barrels) and nine disks at each
end (referred to as end-caps). It comprises 4088 modules each assembled from two pairs of single-
sided silicon micro-strip sensors, mounted back to back with a 40 mrad stereo angle. Each sensor
contains 768 strips at a pitch of 80 μm. The barrel contains 2020 modules made of rectangular
silicon strips sensors with crystal orientation along the crystal axis <111> plus 92 modules made
of sensors with <100> crystal orientation. The end-caps consist of 1976 wedge-shaped and tapered
strips. In the SCT, most of the signal is generated by the holes drifting towards the p-implant strips.
The signal from each strip is amplified and compared with a threshold in the radiation-hard front-
end ABCD chip [4] (a common discriminator threshold corresponding to a charge of 1 fC was used
during data taking).

For each strip, the discriminator output is sampled for 3 consecutive time bins: for the triggered
bunch crossing (BC) as well as the BC before and after the triggered BC. The chip is configured
to register a "hit" depending on the pattern of the three sampled time bins. For cosmic ray running
and for optimising the timing, a hit simply requires a signal in any of the 3 bins. For moderate
luminosity (used up to 2013), the chip is configured for X1X, meaning a signal in at least the
triggered time bin. At very high luminosity, the chips will require 01X, whereby signals in the BC
before the trigger are vetoed. The relative occupancies of the three time bins are used to optimise
the timing of the SCT, so that all hits match the 01X pattern.

3. Occupancy

The occupancy is defined as the number of strips above threshold over the total number of strips. In order to avoid confusion in pattern recognition in a high track multiplicity environment such the one at the LHC, the SCT was designed to minimise the detector occupancy.

For the initial design luminosity of 10^{34} cm^{-2} s^{-1} at a beam-crossing rate of 40 MHz the mean number of interactions per crossing was expected to be 23. In these circumstances, the mean strip occupancy was expected to be less than 1%. In 2012, with an LHC bunch-spacing of 50 ns, the design goals for pile-up were exceeded with no significant loss of tracking efficiency.

From 2015, the LHC will deliver significantly higher pileup which could potentially exceed the bandwidth limitations of the SCT DAQ. The DAQ has therefore been expanded to be able to operate at 100kHz trigger rate with a pileup of ~ 90. The limit within the SCT DAQ is related to the off-detector DAQ system that has been significantly expanded during 2014 to match the same bandwidth capabilities as the from-end chips. Figure 2 shows the mean occupancy of each barrel module as a function of the number of interactions per bunch crossing in minimum-bias *pp* data.
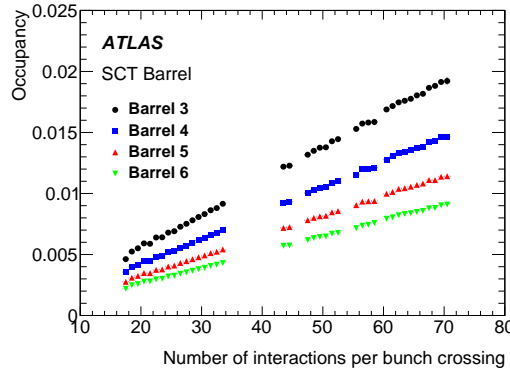
Figure 2: Mean occupancy of each layer of the SCT barrel as a function of the number of interactions per bunch crossing in minimum-bias *pp* data. Values for less than 40 interactions per bunch crossing are from collisions at $\sqrt{s} = 7$ TeV, those for higher values are from special low-luminosity test-runs at $\sqrt{s} = 8$ TeV, which have an occupancy larger by a factor of about 1.03 for the same number of interactions per bunch crossing.

4. Energy loss and particle identification

Although the SCT is not designed to perform measurements of energy loss, dE/dx, and particle identification, some discriminating power is available from the number of time bins above threshold and the number of strips in a cluster. The particle identification is performed using a likelihood method by fitting dE/dx of particles identified as protons, kaons or pions on the basis of dE/dx measured in the pixel detector.

For p$_T$ in the range 400-500 MeV, the tagging efficiency for protons is higher than 90% with a mistag rate lower than 30% for kaons and lower than 4% for pions.

5. Intrinsic hit efficiency

The intrinsic hit efficiency corresponds to the probability of a hit being registered in an operational detector element when a charged particle traverses the sensitive part of the element. It is defined at the ratio of the numbers of recorded hits (clusters) on the tracks with $p_T > 1$ GeV/c to the number of expected hits.
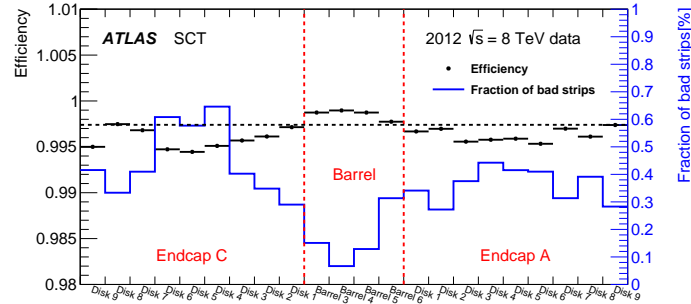
Figure 3: SCT hit tracking efficiency (black) and fraction of disabled strips in each layer (blue line and right-hand axis) measured in $\sqrt{s} = 8$ TeV *pp* collisions.

Figure 3 shows the hit efficiency for each SCT barrel and disk, together with the fraction of non-working strips (dead or noisy) in that layer. The measured efficiency is around 99.9 % for barrel and 99.6 % for end-cap modules and, as expected, it is correlated with the number of disabled strips.

6. Lorentz angle

The presence of the magnetic field affects the drift of the charge carriers inside the detector due to the Lorentz force. This is particularly important for barrel modules where the direction of
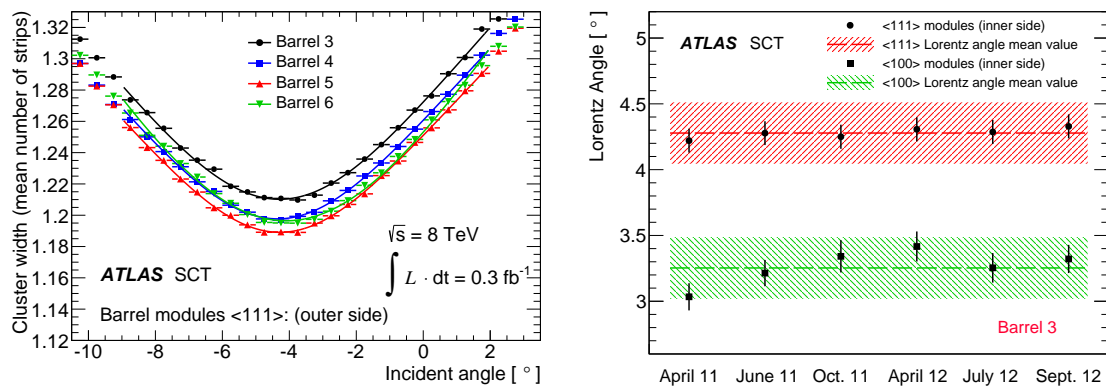
Figure 4: (*left*) cluster-size dependence on the particle incident angle for each SCT barrel for <111> sensors; (*right*) average fitted values of the Lorentz angle for <111> and <100> sensors in the innermost barrel for stable-beam running periods in 2011 and 2012 (the dashed line shows the average over the full 2011 and 2012 datasets, with the correlated systematic uncertainty indicated by the shaded band).

the charge carrier drift is perpendicular to the magnetic field. For end-cap modules, charge carriers drift in a direction almost parallel to the magnetic field, thus no significant effect of the magnetic field is expected.

The Lorentz angle is determined by measuring the dependence of the cluster size on the particle incident angle (figure 4 left). The mean value along the 2011/2012 data taking period (figure 4 right) is $(4.28 \pm 0.23)°$ for $<111>$ modules and $(3.25 \pm 0.23)°$ for $<100>$ modules, showing a variation of no more than $0.1°$.

7. Radiation damage effects

The high radiation doses on silicon sensors result in damage of the bulk silicon and the dielectric layers that can increase the leakage current of the sensor, produce changes to the doping concentration (and hence depletion voltage), and modify the inter-strip capacitance.
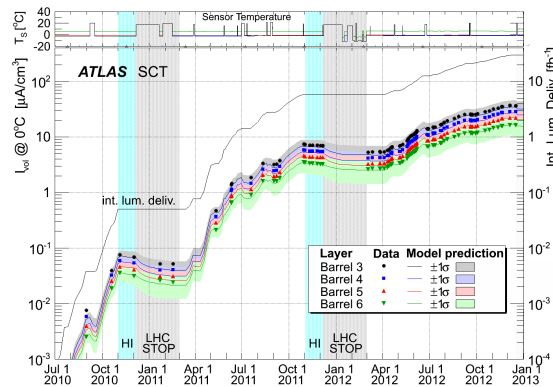
Figure 5: data (points) and Hamburg/Dortmund model predictions (lines with uncertainties shown by the coloured bands) of the leakage current of the four barrel layers. The integrated luminosity and the average sensor temperatures are also shown. The blue shading and label "HI" indicate periods of heavy-ion running, while extended periods with no beam in the LHC, during which the SCT was off, are shaded grey.

The radiation damage can be monitored using the leakage current of the modules that has been measured and found in agreement with the Hamburg/Dortmund [5, 6] model simulated using the FLUKA particle transport code [7, 8] and including self annealing effects based on the different measured sensor temperatures. Figure 5 shows the average leakage current of each layer compared with the prediction that confirms how the radiation fluences are well described by the FLUKA prediction.

The increased leakage current does not affect the SCT detection efficiency as expected, and so far no significant changes in sensor depletion voltages are expected or observed.

8. Conclusions

After three years of operation, the performance of the SCT are well within its design specification with more than 99 % of the detector fully functional. The DAQ system has been significantly expanded in the 2014 to allow the detector to be fully operational even in the high luminosity scenario expected for Run 2.

References

[1] ATLAS Collaboration, *The ATLAS Experiment at the CERN Large Hadron Collider*, JINST **3** (2008), S08003.

[2] ATLAS Collaboration, *The ATLAS Inner Detector commissioning and calibration*, Eur. Phys. J. **C70** (2010), 787 - 821. arXiv:1004.5293.

[3] ATLAS Collaboration, *Operation and performance of the ATLAS semiconductor tracker*, arXiv:1404.7473.

[4] *F. Campabadal et al.*, *Design and performance of the ABCD3TA ASIC for readout of silicon strip detectors in the ATLAS semiconductor tracker*, Nucl. Instrum. Meth. **A 552** (2005) 292.

[5] M. Moll, *Radiation Damage in Silicon Particle Detectors*, Thesis, Universitität Hamburg, 1999. https://mmoll.web.cern.ch/mmoll/thesis/pdf/moll-thesis.pdf .

[6] O. Krasel, *Charge Collection in Irradiated Silicon-Detectors*, Thesis, Universitität Dortmund, 2004. http://d-nb.info/1011531879/34 .

[7] A. Ferrari, P. R. Sala, A. Fasso, and J. Ranft, *FLUKA: A multi-particle transport code (Program version 2005)*, CERN-2005-010, SLAC-R-773, INFN-TC-05-11, http://cdsweb.cern.ch/record/898301.

[8] G. Battistoni et al., *The FLUKA code: description and benchmarking*, AIP Conf. Proc. **896** (2007) 31.

PoS(TIPP2014)334